Aeroelastic modelling of aircraft empennage buffet

O. Levinski *

(Received 8 August 2003)

Abstract

The airframes of high performance aircraft, such as the F/A-18, have suffered from aeroelastic tail buffet problem for many years. This problem is inherent to vortical flows used to generate lift at high angles of attack as they tend to break down causing empennage severe dynamic loading and its premature fatigue failures. The challenges associated with the empennage buffet problem vary from prediction of the nonlinear separated vortical flows about complex configurations to the coupled interaction between the flow and the dynamic response of the tail structure. The paper describes he development and validation of aeroelastic model for the prediction of empennage buffet due to bursting vortices. The multidisciplinary problem of tail buffeting is solved accurately in time using an unsteady vortex model for

*DSTO Platforms Sciences Laboratory Melbourne, Victoria 3207, Australia.
mailto:Oleg.Levinski@dsto.defence.gov.au

See http://anziamj.austms.org.au/V45/CTAC2003/Levi/home.html for this article, Published September 6, 2004. ISSN 1446-8735

prediction of aerodynamic loads and coupled aeroelastic equations for the bending and torsional deflections of the tail which are resolved using the Galerkin method. A dynamic aeroelastic analysis of empennage buffet is performed for a generic delta-wing, twin vertical-tail configuration at high angles of attack. Results of flow simulation indicated that the aeroelastic model is able to predict major unsteady features of the vortex induced buffet loads and the resulting coupled fluid-structure interaction.

Contents

1 Nomenclature

(A)	Aerodynamic loading vector
$[M]$	Mass matrix
$[K]$	Stiffness matrix
$(J-I)$	Number of torsion modes
C_p	Pressure coefficient
EI	Distributed bending stiffness
GJ	Distributed torsional stiffness
I	Number of bending modes
I_θ	Mass moment of inertia
M	Distributed aerodynamic pitch moment
m	Distributed mass
N	Distributed aerodynamic normal force
q_i	Generalised coordinate for bending mode
q_j	Generalised coordinate for torsion mode
$\mathbf{u}$	Flow velocity
w	Dimensionless flow velocity
x_θ	Local distance between the elastic axis and inertial axis
Y	Tail bending deflection
z	Distance from the fixed support along the tail elastic axis
ϕ	Dimensionless velocity potential
ν	Flow viscosity
θ	Tail torsional deflection
ω	Flow vorticity
ψ_i	Free-vibration mode of bending
ψ_j	Free-vibration mode of torsion

2 Introduction

For modern combat aircraft, the ability to fly and manoeuvre at high angles of attack and at high loading conditions gives tactical advantages. For the F/A-18 aircraft the manoeuvrability at very high angles of attack is achieved through a combination of the wing root leading edge extensions (LEXs) and the placement of twin vertical tails. The energetic vortices generated by the highly swept LEXs help to maintain lift during post-stall flight but tend to break down under certain flight conditions causing severe empennage buffeting and its premature fatigue failures. As future military aircraft are also expected to operate at high angles of attack in manoeuvering flight, practical methods are needed to accurately account for the buffet loads.

Although aeroelastic models based on Euler and Navier–Stokes codes can be applied for the simulation of F/A-18 vertical tail buffeting, they require enormous computing resources to perform parametric studies. Even the single computation of a time-accurate solution of F/A-18 tail buffet at certain flight conditions using the above codes is at the very limit of the capabilities of modern supercomputers. Alternatives to computationally intensive Euler and Navier–Stokes codes are vortex-based methods which provide economy in computations by concentrating their efforts in the areas of high vorticity gradients. The vortex methods are particularly suitable for simulation of vorticity dominated regions, such as flow past a LEX.

The purpose of this research is to provide an improvement in aeroelastic analysis capabilities through the application of the unsteady vortex model to the aeroelastic formulation. This includes the modeling of leading edge vortex development and breakdown, and the interaction of a burst vortex flow field with flexible vertical tails. Further improvements such as structural nonlinearities can be easily incorporated in the aeroelastic scheme. However, the emphasis in this research is placed on the aerodynamic model and the solution strategy.

3 Numerical method

A general approach to the computation of the response of a structure to dynamic loads is provided by energy methods, see Meirovitch [1]. In such methods, the solution is derived by describing the dynamic response in terms of small displacements about equilibrium points.

3.1 Aeroelastic equations

To facilitate the development of the approach, the vertical tail is represented as a flexible cantilevered beam with rigidly fixed root and rigid cross-section. The tail bending $Y(z,t)$ and torsional $\theta(z,t)$ deflections occur about an elastic axis that is not necessary coincident with the inertial axis.

The linearised dynamic equations for the coupled bending and torsional vibrations of the vertical tail are

$$m(z)\frac{\partial^2 Y}{\partial t^2} + m(z)\,x_\theta(z)\frac{\partial^2 \theta}{\partial t^2} + \frac{\partial^2}{\partial z^2}\left(EI(z)\frac{\partial^2 Y}{\partial z^2}\right) = N(z,t)\,, \quad (1)$$

$$I_\theta(z)\frac{\partial \theta}{\partial t} + m(z)\,x_\theta(z)\frac{\partial^2 Y}{\partial t^2} - \frac{\partial}{\partial z}\left(GJ(z)\frac{\partial \theta}{\partial z}\right) = M(z,t)\,. \quad (2)$$

For a flexible vertical tail represented as a cantilevered beam, the geometrical and natural boundary conditions on Y and θ are

$$Y(0,t) = \frac{\partial Y(0,t)}{\partial z} = \frac{\partial^2 Y(L,t)}{\partial z^2} = \frac{\partial}{\partial z}\left[EI(L)\frac{\partial^2 Y(L,t)}{\partial z^2}\right] = 0\,, \quad (3)$$

and

$$\theta(0,t) = \frac{\partial \theta(L,t)}{\partial z} = 0\,. \quad (4)$$

Solve the above equations by an expansion of the dependent variables in terms of the natural free vibration modes of the system, see Meirovitch [1].

Here,

$$Y(z,t) = \sum_{i=1}^{I} \psi_i(z)\, q_i(t) \quad \text{and} \quad \theta(z,t) = \sum_{j=I+1}^{J} \psi_j(z)\, q_j(t)\ . \tag{5}$$

Substituting these expansions into Equations (1) and (2) and using the Galerkin method, along with integration by parts and imposing the boundary conditions (3) and (4), we get the following equations for the generalised coordinates q_i and q_j in matrix form

$$\begin{bmatrix} M_{11} & M_{12} \\ M_{21} & M_{22} \end{bmatrix} \begin{bmatrix} \frac{\partial^2 q_i}{\partial t^2} \\ \frac{\partial^2 q_j}{\partial t^2} \end{bmatrix} + \begin{bmatrix} K_{11} & K_{12} \\ K_{21} & K_{22} \end{bmatrix} \begin{bmatrix} q_i \\ q_j \end{bmatrix} = \begin{bmatrix} A_i \\ A_j \end{bmatrix}\ . \tag{6}$$

see Strganac [2]. Note, that the above equations of motion are coupled both inertially and aerodynamically, as the sectional centre of gravity and elastic axis are not generally coincident and the aerodynamic loads are motion dependent.

3.2 Unsteady aerodynamic model

The equations of motion (6) describing the dynamic response of the system require an aerodynamic model that is able to predict unsteady buffet loads on a vertical tail simultaneously with the motion. Levinski [3, 4] showed that the vortex model is able to predict the onset of leading edge vortex breakdown past a delta wing, twin-tail configuration and qualitatively describe its unsteady behaviour. Also, spatial and temporal characteristics of unsteady buffet pressures arising on the rigid tail were found to be in qualitative agreement with available experimental data.

Vortex methods simulate the unsteady fluid flows under the assumption of nonlinear dynamics of vorticity, so fluid flows at high Reynolds numbers are simulated by regions of concentrated vorticity embedded in irrotational

fluid. The vorticity transport equation governs incompressible fluid flows subjected only to irrotational body forces:

$$\frac{\partial \omega}{\partial t} + (\mathbf{u} \cdot \nabla)\,\omega = \omega \cdot \nabla \mathbf{u} + \nu \nabla^2 \omega\,, \tag{7}$$

where it is assumed that the divergences of the velocity and vorticity are zero. This equation represents simultaneous convection and diffusion of vorticity in the flow field as well as concentration of vorticity due to vortex filament stretching. The solution is obtained using the widely adopted fractional step method, which simulates the convection and the diffusion processes sequentially rather than simultaneously, see Leonard [5]. This is achieved by solving Euler's equations by the vortex method and using the proper numerical technique to model the diffusion equation.

The evolution of vortex elements is tracked numerically in a Lagrangian or hybrid Euler–Lagrangian reference frame. The required local velocities are computed as the solution of Poisson's equation for the velocity field in terms of Biot–Savart integrals. The result is a nonlinear system of ordinary differential equations giving the temporary evolution of vorticity coordinates. Detailed description of the unsteady vortex method can be found in [4, 6].

To complete the model, one should account for the process of vorticity production at the body surface to define the initial distribution of vorticity. Within the scope of vortex theory, this involves full treatment of boundary layer vorticity by simulating the process of its creation at the wall and its subsequent convection and viscous diffusion. As an alternative to such a computationally intensive algorithm I allow the boundary layer to separate only at a finite number of separation points, assuming potential flow modelling for the rest of the body. Here, the vorticity diffusion and convection activities within the body boundary layer are completely ignored therefore substantially reducing the computational effort. It is implicitly assumed in such an approach that the places of separation are known a priori and fixed at some locations at the body surface. This approximation, as well as the assumption of fully attached flow on the rest of the body surface, is com-

monly used in inviscid flow calculations. Following this simplified technique an accurate prediction of overall aerodynamic characteristic may be obtained especially for sharp edged bluff bodies.

Using the Cauchy–Lagrange equation [6] for inviscid incompressible flow, the unsteady pressure coefficient

$$C_p(\mathbf{r},t) = 1 - w^2(\mathbf{r},t) - 2\frac{\partial\phi(\mathbf{r},t)}{\partial t}. \tag{8}$$

A distribution of unsteady pressure coefficients are integrated over the whole body surface to obtain the instantaneous values of aerodynamic forces $N(z,t)$ and moments $M(z,t)$ required for the solution of the equations of motion (6).

3.3 Numerical solution of aeroelastic equations

Solution of the aeroelastic equations (6) in the time domain presents a challenge since the aerodynamic loads depend on the tail motion, yet the tail motion cannot be determined unless the aerodynamic loads are known. Following Strganac [2], an iterative numerical integration scheme that accounts for the interaction between the aerodynamic loads and tail dynamic response is developed which determines the motion of the structure and the motion-dependent aerodynamic loads simultaneously. The method is based on a fourth-order Hamming's predictor-corrector method, see Carnahan et al. [7]. An advantage of the predictor-corrector method is that it does not subdivide a time step of integration, as do other numerical integration techniques, such as the Runge–Kutta method, providing substantial economy of computations.

For each time step, integration of the equation of motion by Hamming's method begins with the computation of the fluid flow and convection of wake vorticity to the new force-free position from the position generated at the end of the last time step. When the new tail geometry is computed, the

aerodynamic loads are updated, and convergence of both the state variables and aerodynamic loads is checked. If convergence is not achieved, the state variables are corrected and new aerodynamic loads are determined. Here, only unsteady aerodynamic loads are updated each time the state variables are predicted or corrected. This process is repeated until convergence of the loads and tail motion is achieved while maintaining the flow field in a fixed position.

4 Computation of vertical tail dynamic response

Wheras an ultimate aim of this work is to investigate the F/A-18 empennage buffet, Levinski [4] showed that the vertical tail buffet problem could be simulated efficiently using a generic delta wing, twin vertical-tail configuration. This simple configuration contains all the pertinent physics involved in the development and burst of a leading-edge vortex and its subsequent interaction with the vertical tails. In this way, the major characteristics of the vertical tail buffet are investigated without complications associated with simulation of the flow over the complete F/A-18 aircraft.

4.1 Computational model

The same delta wing, twin vertical-tail configuration as used in the buffet study of Levinski [4] is employed to computationally simulate the vertical tail dynamic response. It consists of a sharp-edged, 76 degree leading edge sweep delta wing and swept-back F/A-18 twin tails. Both the delta wing and twin tails are of zero thickness. Each of the tails is of aspect ratio 1.2 with the root chord length of 0.4 and a tip chord length of 0.159, based on the delta wing root chord. The tails are cantilevered on the upper surface of

a trailing edge extension of the delta wing and have a sweep back angle of 35 degrees for a quarter-chord span wise line. The tip of each tail is inclined outboard such that dihedral angle between the two tails is 40 degrees. The span wise separation distance between the tails at the root is 50% of the delta wing span.

The numerical simulation procedure requires a discretisation of the computational model, thus a total of 2986 closed vortex rings, or panels, are used for spatial discretisation of the delta wing, trailing edge extension and twin vertical tails. A unit aspect ratio delta wing is modelled using 2178 quadrilateral vortex panels. The vortex system of the trailing edge extension continues the discretisation pattern of the delta wing and is represented by 416 rectangular panels while 196 trapezoidal panels model each of the vertical tails.

Each of the elastic vertical tails of the computational model is treated as a swept back beam which is allowed to oscillate in bending and torsion modes. In the present study of coupled bending-torsion response, the distance between the elastic axis and the inertia axis for each of the tails is set equal to 0.04 based on delta wing root chord.

4.2 Test conditions

Based on the critical dynamic response region defined in [8], the test conditions for the dynamic aeroelastic model were selected to vary between 20 and 40 degrees angle of attack at 12 kPa dynamic pressure and altitude of 3,000 m as these conditions are most important in vertical tail buffet studies. During the simulations, the fluid was started impulsively and computation was carried out for 300 time steps with a dimensionless time increment of $\Delta t = 0.012$ that allows the vortex wake to travel 8.6 tail root chord lengths at the rate of the free-stream velocity. This computational time span is deemed to be adequate to obtain a fully developed vortex wake allowing the unsteady buffet loads to be considered as random and stationary in a statistical sense.

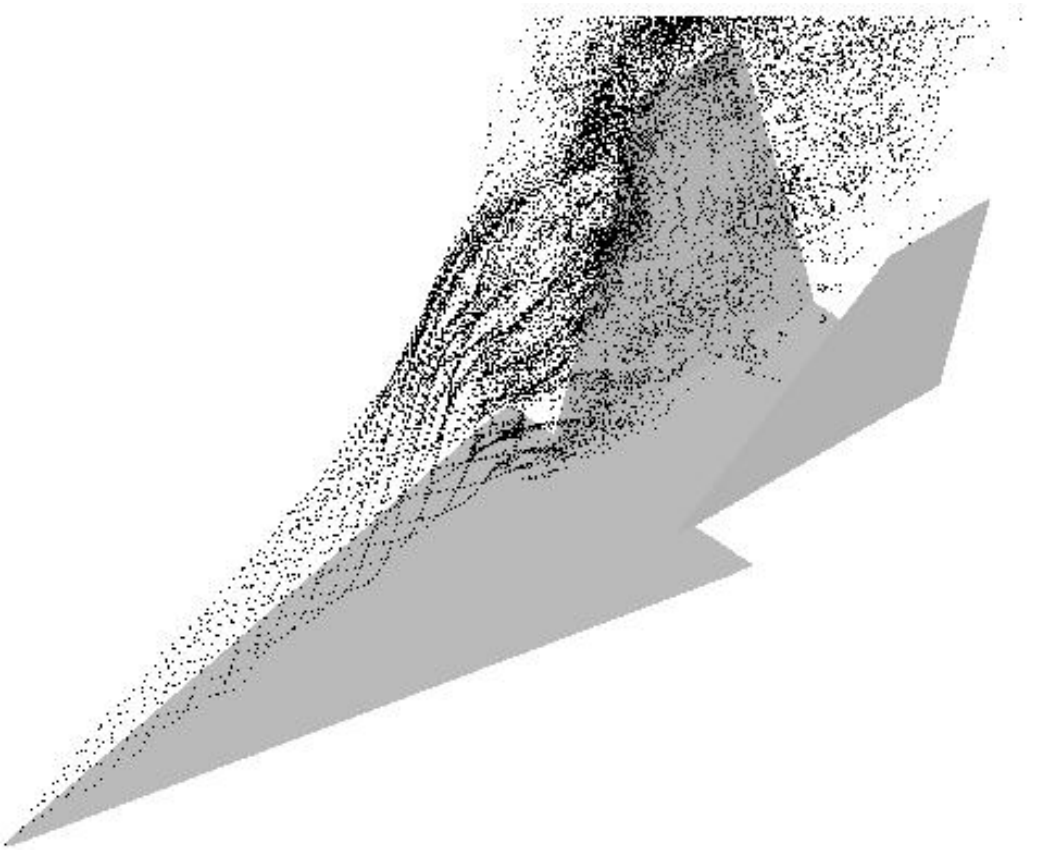

FIGURE 1: Particle traces of the leading edge vortex core at 30 degrees angle of attack

4.3 Vortex wake structure

Details of the flow development over the delta wing, twin vertical-tail configuration are provided in Figure 1 where the leading edge vortex is visualised by particle traces, which are plotted for several consecutive time steps. See that the vortex model reproduces the leading edge vortex roll-up, which is typical of the flow over delta wings. This leading edge vortex expands in a continuous manner while convecting downstream. The vortex core is initially intact and stable as indicated by the coinciding particle traces. However, at some point downstream, the growing scatter of the particle traces reveals onset of instability and perturbation of the vortex core that results in a highly disturbed wake, which convects downstream undergoing gradual expansion.

4.4 Vertical tail buffet loading

The magnitude and frequency content of instantaneous pressure fluctuations on the tail surface are the most important characteristics of tail buffet. The differential (buffet) pressure is estimated from time histories of surface pressure fluctuations as the difference between the inner surface pressure values and outer surface pressure values on the tail. The values of unsteady differential pressures are integrated over the vertical tail surface to give components of aerodynamic load coefficients. The unsteady pressure and loads coefficients are reduced to root-mean-square (RMS) and power spectral density (PSD) forms. The peak power and the dominant frequency of the unsteady buffet loads are determined from their PSD plots.

4.4.1 Magnitude of buffet pressures

It is common in vertical tail buffet studies to examine and compare characteristics of surface pressure fluctuations measured at the 45% chord and

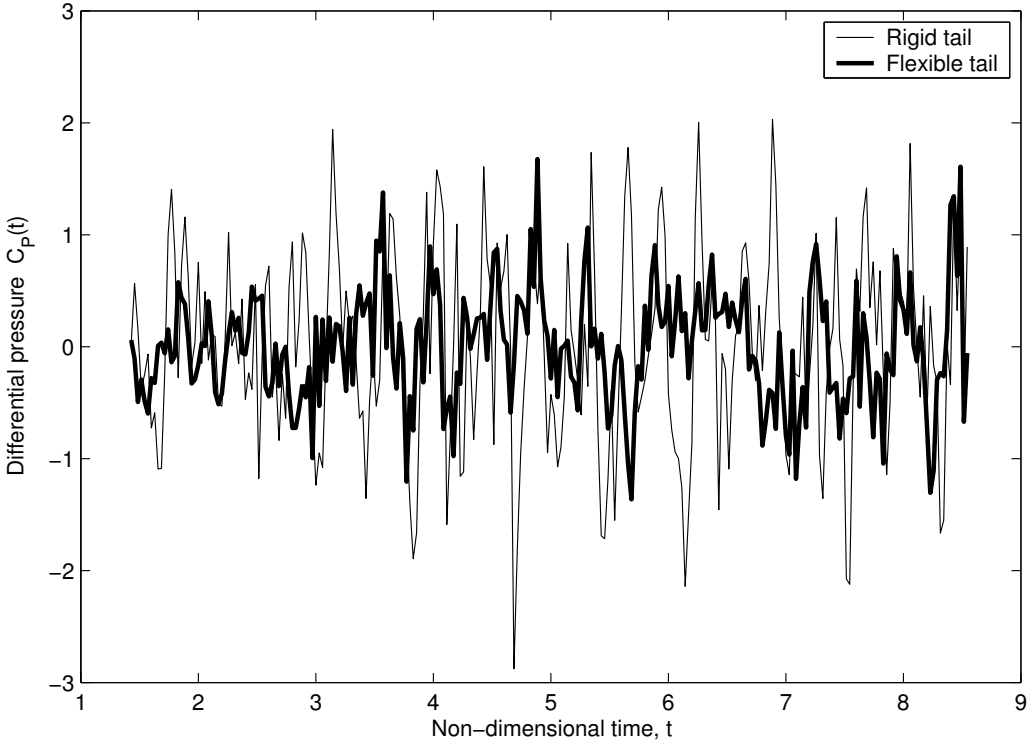

FIGURE 2: Time history of differential pressure coefficient at 45% chord and 60% span location

60% span location on the vertical tail. It provides a common base for comparison of the results of various experimental and numerical tail buffet studies. Figure 2 shows a computed time history of the differential pressure fluctuations at 45% chord and 60% span location obtained on the flexible vertical tail at 30 degrees angle of attack, and is also accompanied by computational results obtained on a rigid tail. See that for both the rigid and flexible tails, the differential pressure coefficients fluctuate substantially and exhibit oscillatory motion with large random fluctuations about a local mean value. However, the magnitude of differential pressure fluctuations on the flexible vertical tail is lower compared with the rigid tail case. This reduction of magnitude of buffet pressure fluctuations measured on the flexible tail is consistent with the trends obtained from experimental and flight test data [9].

Variation of RMS differential pressure fluctuations obtained at 45% chord and 60% span location on rigid and flexible tails, and a full-scale wind tunnel test of F/A-18 tail buffet [10] at different angles of attack is presented in Figure 3: the RMS buffet pressure fluctuations measured on the flexible tail are lower than the rigid tail values for all the angles of attack but still higher than full-scale test data. Despite both the rigid and flexible tail RMS buffet pressures over-predicting measured data, the overall reduction of buffet pressure values representing the effect of tail flexibility matches experimentally observed trends.

4.4.2 Spectral content of buffet pressures

Figure 4 shows the spectral content of the differential pressure fluctuations at 30 degrees angle of attack at the 45% chord, 60% span location for rigid and flexible tail models. On the rigid tail the differential pressure contains energy over a relatively narrow frequency band with centre frequency of 2.9 corresponding to the dominant frequency of vortex breakdown flow. This differential pressure power peak occurs at about the same frequency values across the whole surface of the rigid tail. However, power spectral densities of

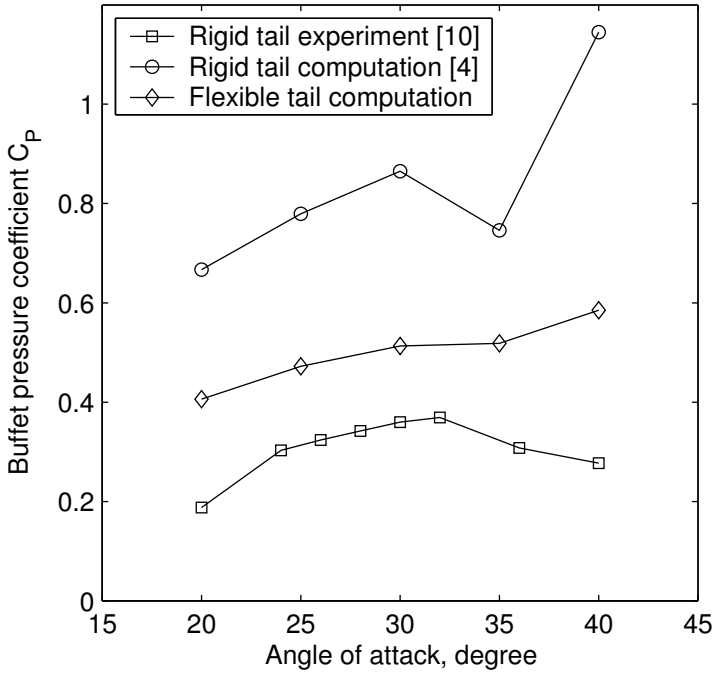

FIGURE 3: Comparison of RMS differential pressure values at various angles of attack at 60% span, 45% chord location on the tail

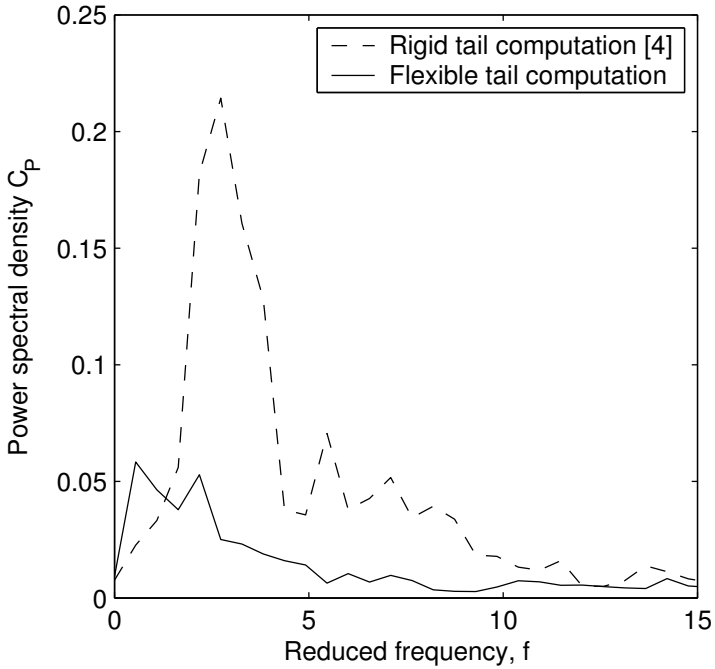

FIGURE 4: Power spectral density of differential pressure fluctuations at 45% chord and 60% span location on the tail

considerably lower magnitudes are predicted for the flexible tail model where two distinct peaks are now aligned with the fundamental frequencies of the tail bending and torsion modes. The presence of pressure fluctuations near the tail natural frequencies is the result of coupled flow-structure interaction where elastic tail response modifies the differential pressure fluctuations initially caused by turbulent vortex breakdown alone.

Random fluctuations of the buffet pressures are caused by interaction of the highly turbulent leading edge vortex flow with the vortex system of the twin vertical tails. The leading edge vortex breakdown causes flow deceleration and the leading edge vorticity tends to concentrate in the region near the twin tails, gradually building up a vortex cloud. The process of formation and destruction of the vortex clouds interacting with the tail vortex system drives the oscillatory behaviour of the buffet loads. These drifting clouds of scattered vorticity are also subjected to random-like motion caused by vortices bouncing back off the tail surface that also imposes a certain degree of randomness to the surface pressure distribution.

The periodicity of the vortex cloud formation determines the dominant frequencies of buffeting flow. However, this is further affected by the dynamic response of the flexible vertical tails. The vertical tail deflections change the location and shape of the vortex breakdown flow that modifies pressure distribution on the tails as well as its frequency content by the appearance of motion-driven pressure fluctuations. The resulting buffet pressure magnitudes and frequency content depend on intensity and coupling of both the unsteady aerodynamic loads arising from the leading edge vortex burst and those caused by the vibration of the tail.

4.4.3 RMS pressure distribution

A contour plot of calculated RMS differential pressure fluctuations on a flexible vertical tail at 30 degrees angle of attack is presented in Figure 5 and accompanied by rigid tail results to investigate variation of buffet pressure

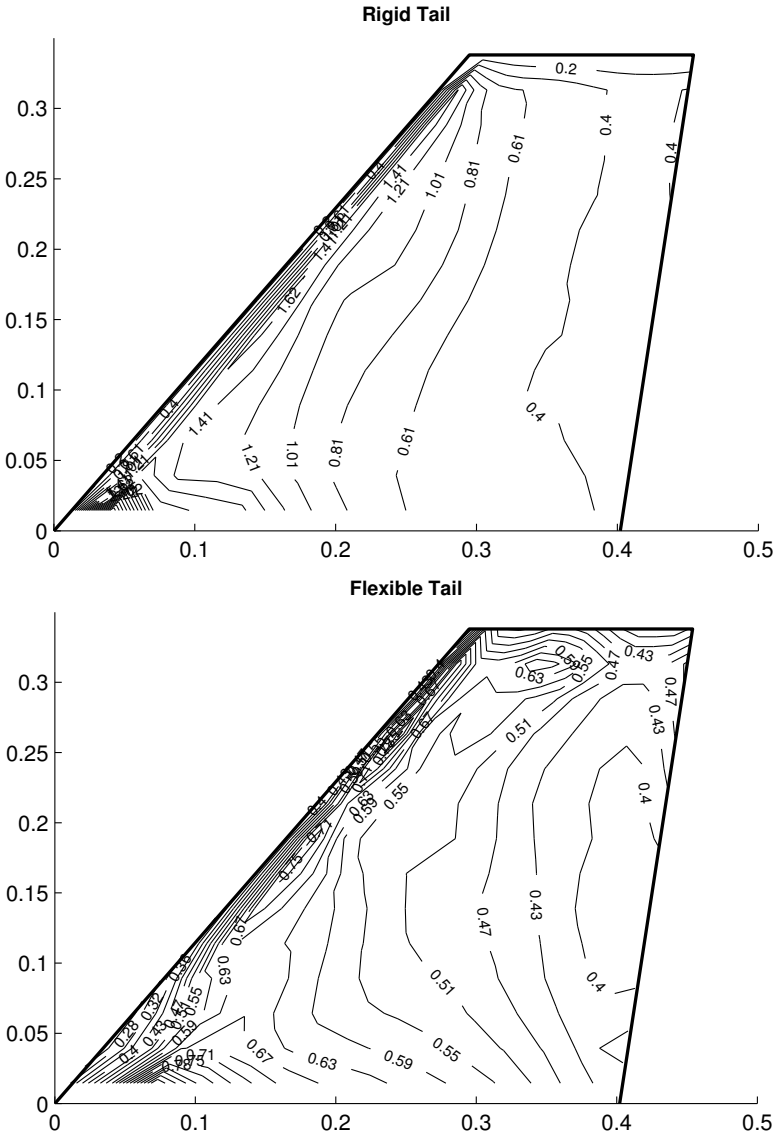

FIGURE 5: Distribution of RMS differential pressure over the tail at 30 degrees angle of attack.

distribution. On the flexible tail, the pressure fluctuations are higher at the leading edge as this area is the closest to the breakdown location, whereas the pressure fluctuations tend to decrease towards the trailing edge. However, on a rigid tail, the decrease in differential pressure towards the trailing edge is rather uniform while on a flexible tail the pattern is more complex and irregular. Although the general trend of decrease of buffet pressure RMS towards the trailing edge is present for most of the tail surface, the pressure field is obviously affected by the tail dynamic response, especially at those parts of the tail surface where deflections are the largest.

5 Conclusions

A time-accurate dynamic aeroelastic analysis of empennage buffet has been performed for a generic delta wing, twin vertical-tail configuration using an unsteady vortex model for prediction of aerodynamic loads and coupled aeroelastic equations for the bending and torsional deflections of the tail. The numerical solution is able to predict onset of the vortex burst and qualitatively describe the characteristics of unsteady buffet loads on the vertical tail.

It was found that the magnitude of differential pressure fluctuations on a flexible vertical tail is lower compared to the rigid tail case. Despite both the rigid and flexible tail models over-predicting the measured data, the overall reduction of buffet pressure values representing the effect of tail flexibility matches experimentally observed trends.

Comparison of computational results with available wind-tunnel and flight test data of F/A-18 tail buffet revealed that the dynamic aeroelastic model performed reasonably well in simulating the spatial and temporal characteristics of the buffet loads. Computational analysis of the flexible tail showed a difference in buffet loading when compared to the rigid tail model. Here, both the tail bending and torsion modes had a noticeable contribution to the buffet load magnitude and frequency content and this emphasises the need

to account for tail flexibility during computations of the empennage buffet.

References

[1] L. Meirovitch. *Computational Methods in Structural Dynamics* Sijtohoff & Noordhoff International Publishers, Alphen ann den Rijn, The Netherlands. 1980. C985

[2] T. W. Strganac. *A Numerical Model of Unsteady, Subsonic Aeroelastic Behavior*, NASA-TM-100487, December 1987. C986, C988

[3] O. Levinski. *Review of Vortex Methods for Simulation of Vortex Breakdown*, Aeronautical and Maritime Research Laboratory, DSTO-TR-1211, 2001. C986

[4] O. Levinski. *Prediction of Buffet Loads on Twin Vertical Tails Using a Vortex Method*, Aeronautical and Maritime Research Laboratory, DSTO-RR-0217, 2001. C986, C987, C989

[5] A. Leonard. Vortex Methods for Flow Simulation. *J. Comp Phys.* **37, No. 3** 289–335, 1980. C987

[6] S. M. Belotserkovskii and M. I. Nisht. Modelling of Turbulent Wakes in Ideal Fluids (Separated Flow Over Bluff Bodies), *Fluid Mech.-Research.* **7, No. 1** 102–115, 1978. C987, C988

[7] B. Carnahan, H. A. Luther and J. P. Wilkes *Applied Numerical Methods*, John Wiley & Sons, Inc., New York, 1969. C988

[8] C. R. Mouser, D. P. Conser *F/A-18 IFOSTP FT46 Pre Block 1 and Post Block 5 Dynamic Strain Survey Testing and Results*, Australian Department of Defence, DSTO, Aeronautical and Maritime Research Laboratory, DSTO-TR-1218, 2001. C990

[9] L. A. Meyn, K. D. James, and R. J. Geenen *Correlation of F/A-18 Tail Buffet Results*, High-Alpha Projects & Technology Conference, NASA Dryden Flight Research Center, July 1994. C994

[10] C. L. Pettit, D. L. Brown, E. Pendleton, Wind Tunnel Tests of Full-Scale F/A-18 Twin Tail Buffet: A Summary of Pressure and Response Measurements, *AIAA Paper* 94-3476, 1994. C994